ANTIOXIDANTS & REDOX SIGNALING
Volume 31, Number 6, 2019

DOI: 10.1089/ars.2018.7642

Discoveries

FORUM ORIGINAL RESEARCH COMMUNICATION

Redox Regulation of the Mitochondrial Quality Control Protease Oma1

Iryna Bohovych,[1] Jonathan V. Dietz,[1] Samantha Swenson,[1,*] Nataliya Zahayko,[1] and Oleh Khalimonchuk[1–4]

Abstract

Aims: Normal mitochondrial function and integrity are crucial for cellular physiology. Given the paramount role of mitochondrial quality control proteases in these processes, our study focused on investigating mechanisms by which the activity of a key quality control protease Oma1 is regulated under normal conditions and in response to homeostatic insults.
Results: Oma1 was found to be a redox-dependent protein that exists in a semi-oxidized state in yeast and mammalian mitochondria. Biochemical and genetic analyses provide evidence that activity and stability of the Oma1 oligomeric complex can be dynamically tuned in a reduction/oxidation-sensitive manner. Mechanistically, these features appear to be mediated by two intermembrane space (IMS)-exposed highly conserved cysteine residues, Cys^{272} and Cys^{332}. These residues form a disulfide bond, which likely plays a structural role and influences conformational stability and activity of the Oma1 high-mass complex. Finally, in line with these findings, engineered Oma1 substrate is shown to engage with the protease in a redox-sensitive manner.
Innovation: This study provides new insights into the function of the Oma1 protease, a central controller of mitochondrial membrane homeostasis and dynamics, and reveals the novel conserved mechanism of the redox-dependent regulation of Oma1.
Conclusion: Disulfide bonds formed by IMS-exposed residues Cys^{272} and Cys^{332} play an important evolutionarily conserved role in the regulation of Oma1 function. We propose that the redox status of these cysteines may act as a redox-tunable switch to optimize Oma1 proteolytic function for specific cellular conditions or homeostatic challenges. *Antioxid. Redox Signal.* 31, 429–443.

Keywords: mitochondria, mitochondrial quality control, proteases, Oma1, redox regulation

Introduction

NORMAL MITOCHONDRIAL FUNCTIONING and adequate responses to homeostatic challenges are essential for cellular physiology and are regulated by multiple processes. One mechanism includes mitochondrial membrane proteases—a group of highly conserved enzymes that regulate a variety of vital mitochondrial functions, including energy conversion, mitochondrial dynamics, and inner mitochondrial membrane (IM) homeostasis [reviewed in Refs. (6, 11, 28, 33)]. The IM protease Oma1 is a intermembrane space (IMS)-facing, ATP-independent metallopeptidase that has recently emerged as one of the central regulators of the processes just described (2, 21, 34). For example, in higher eukaryotes, Oma1 mediates proteolytic conversion of the guanosine triphosphatase, Opa1, on cellular insults, thereby propelling fragmentation of the mitochondrial network (11, 16, 17, 20)—an event crucial for cellular physiology and processes such as mitophagy and apoptosis (21, 36). Likewise—even though its substrate repertoire remains to be determined—stress-promoted action of yeast Oma1 is required to cope with homeostatic challenges such as mitochondrial uncoupling or oxidative stress (7). Oma1 is also known to perform protein quality control functions (7, 22, 24, 32, 37) and mediate the

[1]Department of Biochemistry, University of Nebraska-Lincoln, Lincoln, Nebraska.
[2]Nebraska Redox Biology Center, University of Nebraska-Lincoln, Lincoln, Nebraska.
[3]Center for Integrated Biomolecular Communication, University of Nebraska-Lincoln, Lincoln, Nebraska.
[4]Fred & Pamela Buffett Cancer Center, University of Nebraska Medical Center, Omaha, Nebraska.
*Current affiliation: Department of Genetics, Cell Biology and Anatomy, University of Nebraska Medical Center, Omaha, Nebraska.

Innovation

Many cellular processes are critically dependent on normal mitochondrial function and multiple quality control mechanisms are in place to ensure the organelle's fidelity. Here, we demonstrate that a key mitochondrial quality control protease Oma1 is a redox-dependent protein, the reduction-oxidation modifications of which may influence its biochemical properties and function. Our study establishes a mechanistic framework for the identification of molecular determinants of substrate recognition and redox-tuning of Oma1. We propose that the redox status of these cysteines may act as a conserved redox-regulated switch to optimize Oma1 proteolytic function for specific cellular conditions.

stability of respiratory supercomplexes, thereby influencing mitochondrial energy metabolism (8, 14).

The protease is largely dormant under normal physiological conditions, but it becomes rapidly activated by various stress stimuli such as loss of mitochondrial membrane potential, metabolic crisis, heat, and oxidative insults (11, 13, 16, 17, 20). Although its stress-activation mechanism remains obscure, several reports suggested that Oma1 activation is a post-translational process that involves conformational changes within the homo-oligomeric Oma1 complex (7) and have identified several molecular determinants that are important for the protease's activation (13, 17, 35, 43), including the enzyme's conserved C-terminal region (7). By analogy with the other known proteolytic enzymes, such behavior suggests that the protease's activity could be a subject of precise regulatory control *via* a conserved mechanism. Indeed, several studies in mammalian cell culture proposed several regulatory mechanisms, including an autocatalytic cleavage model (3, 43) and stress-induced processing by the ATP-dependent protease Yme1 (35) or the m-AAA [matrix-oriented ATPase associated with various cellular activities (AAA)] protease (13). However, these processes appear to be more evolutionarily recent and specific to higher eukaryotes (3, 7). Moreover, being an evolutionary descendant of the ATP-poor bacterial periplasmic space (30), the IMS is likely to employ additional strategies to regulate its proteome. As such, a deeper understanding of mechanisms that control Oma1 activity under physiological and stress conditions is needed.

In this study, we identified two evolutionarily conserved cysteine residues that influence Oma1 activation and stability. We show that Cys^{332} is crucial for stability and stress-activation of the Oma1 complex. We further demonstrate that mutation of the conserved Cys^{272} stabilizes the C332A mutant form of Oma1, thereby yielding a functional protease complex, which, however, has an altered conformational state. Further analyses in the yeast model indicate that these two residues exist in the oxidized state and suggest that disulfide bonds involving residues Cys^{272} and Cys^{332} are likely to play an important evolutionarily conserved role in the regulation of Oma1 function. The human Oma1 appears to follow the same trend. These data support a model wherein the redox status of these cysteines may act as a redox-tunable switch to optimize Oma1 proteolytic function for specific cellular challenges.

Results

Oma1 exists in a semi-oxidized state and is activated by prolonged hypoxia

To further understand molecular determinants of Oma1 stress-activation, we surveyed for additional stress conditions that may trigger Oma1 activation by using a previously developed proxy assay, wherein changes in the stability of the ~250 kDa Oma1 high-mass complex stability by blue native gel electrophoresis (BN-PAGE) reflect activation of the enzyme (7, 24). In line with previous reports, we observed that the Oma1 oligomer was more labile in mitochondrial lysates from cells stressed with 1 m*M* hydrogen peroxide (H_2O_2) for 1 h—a condition that models an extreme acute oxidative insult—as compared with an untreated control (Fig. 1A, lanes 1 and 2). In contrast, acute osmotic challenge with 1 *M* sodium chloride (NaCl) did not result in Oma1 activation, as reflected by unaltered stability of the Oma1 complex (Fig. 1A, lanes 5 and 6). Intriguingly, we observed that the Oma1 high-mass complex from cells cultured at 1% oxygen was markedly destabilized by BN-PAGE as compared with the complex from control cells grown under normoxic conditions (Fig. 1A, lanes 3 and 4). The steady-state levels of the protease were comparable in each case. Interestingly, we repeatedly noted the appearance of an additional, slightly heavier Oma1-Myc-specific band in the hypoxia-cultured samples (Fig. 1A).

These observations, and the fact that prolonged hypoxia is not associated with enhanced generation of reactive oxygen species (18), prompted us to hypothesize that Oma1 could be responding to changes in the oxygen levels and/or a mitochondrial redox environment. To test this hypothesis, we first sought to determine the redox state of Oma1 under normal physiological conditions. To this end, whole-cell lysates of cells expressing Myc-tagged Oma1 were incubated with the thiol-modifying chemical methyl-polyethylene glycol maleimide 24 [$mm(PEG)_{24}$], which on its binding to free thiol groups increases the molecular weight of the protein in question, thereby retarding the protein's electrophoretic mobility on a nonreducing polyacrylamide gel. We found that Oma1 was partially modified by $mm(PEG)_{24}$ when compared with tris(2-carboxyethyl)phosphine (TCEP)-pretreated (fully reduced) or diamide-pretreated (fully oxidized) variants (Fig. 1B), which indicates that Oma1 contains both reduced and oxidized cysteines under basal conditions. Remarkably, $mm(PEG)_{24}$ modification analysis of human OMA1 in HEK293 cells yielded similar results (Fig. 1C), indicating that the presence of disulfide bond(s) is likely an evolutionarily conserved feature of Oma1. Together, these data suggest that Oma1 might be a subject to thiol-oxidative modifications, which could potentially influence its biochemical properties and function. Interestingly, however, we found that the oxidation state of the protease remained largely unchanged in cells acutely challenged with known stress-activators of Oma1, H_2O_2 or an ionophore carbonyl cyanide m-chlorophenyl hydrazone (CCCP) (Fig. 1D and Supplementary Fig. S1), suggesting that its redox status is probably not significantly altered on the enzyme's activation by these stimuli.

Conserved Cys^{272} and Cys^{332} residues mediate the semi-oxidized state of Oma1 and are important for its stability and function

Oma1 harbors several conserved cysteine residues that may be contributing to its semi-oxidized state. Because the

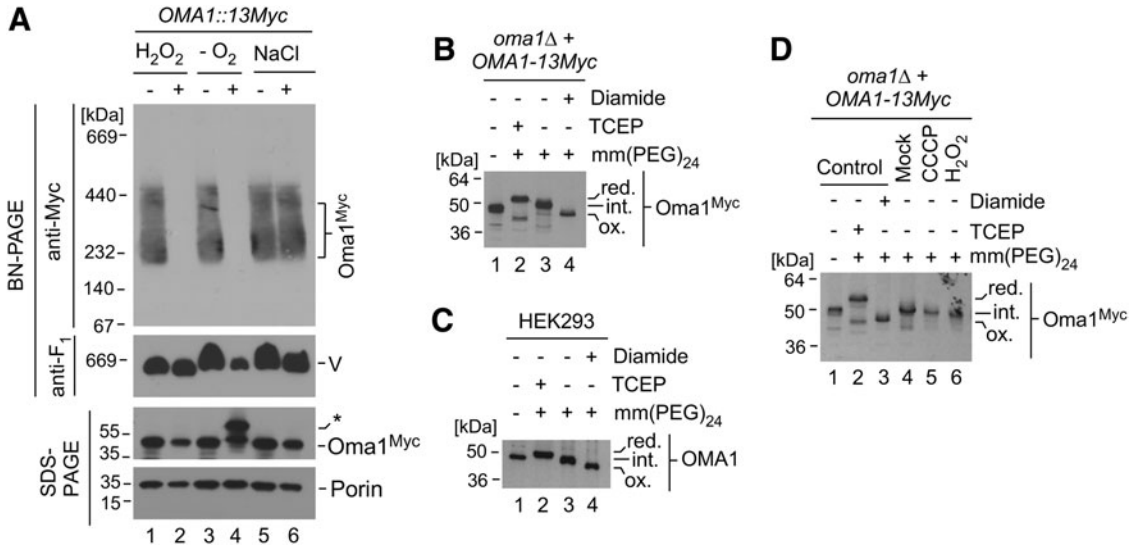

FIG. 1. ***In vivo*** **redox state of Oma1. (A)** Mitochondria were isolated from Oma1-13Myc chromosomally tagged cells that were mock-treated or challenged with 1 m*M* H_2O_2 (acute treatment for 2 h), anoxia ($-O_2$; incubation under 1% O_2 atmosphere for 16 h), or 1 *M* NaCl (acute treatment for 2 h). Seventy micrograms of isolated organelles were lysed in buffer containing 1% digitonin and analyzed by BN-PAGE. The Oma1-13xMyc complexes and monomeric form of respiratory complex V (loading control) were detected by immunoblotting with anti-Myc antibody and anti-F_1 serum, respectively. *Bottom panel*: steady-state levels of indicated proteins were assessed by SDS-PAGE analysis of 15 μg of isolated mitochondria with respective antibodies. *Asterisk* indicates additional Oma1-13xMyc-related band that appears under low-oxygen condition. **(B)** After the precipitation with TCA to prevent cysteine oxidation, denaturation with SDS, and treatment with or without 20 m*M* TCEP (reductant) or 5 m*M* diamide (oxidant), 50 μg of mitochondrial proteins from *oma1*Δ cells expressing Oma1-13xMyc was incubated with alkylating agent $mm(PEG)_{24}$ and analyzed by Western blot. Thiol-specific modification of proteins by $mm(PEG)_{24}$ alters their electrophoretic mobility, wherein migration of a thiol-containing protein is retarded relative to that of unmodified protein. Electrophoretic mobility of $mm(PEG)_{24}$-modified Oma1 was compared with the migration patterns of fully reduced (TCEP-treated) and fully oxidized (diamide-treated; Ox.) forms of the protein. Under conditions tested, Oma1 exhibits an intermediate (Int.) migration profile, thus reflecting the presence of both reduced and oxidized cysteine residues. **(C)** Mitochondrial proteins from HEK293 human embryonic kidney cells were analyzed as in B using antibody against human OMA1. **(D)** Mitochondria from the indicated cells cultured under normal conditions (Mock) or challenged with 1 m*M* H_2O_2 for 2 h or 45 μ*M* CCCP for 2 h were modified and analyzed as described in **(B)**. BN-PAGE, blue-native gel electrophoresis; CCCP, carbonyl cyanide m-chlorophenyl hydrazone; H_2O_2, hydrogen peroxide; $mm(PEG)_{24}$, methyl-polyethylene glycol maleimide 24; NaCl, sodium chloride; SDS-PAGE, sodium dodecyl sulfate–polyacrylamide gel electrophoresis; TCA, trichloroacetic acid; TCEP, tris(2-carboxyethyl)phosphine.

IMS is a well-recognized redox-active mitochondrial subcompartment, we focused our attention on two cysteine residues facing the IMS, Cys^{272} and Cys^{332} (Fig. 2A, B). These cysteine residues are highly conserved among eukaryotes, and mutations in Cys^{332} have been previously shown to affect Oma1 function (7). To better understand the role of these residues in Oma1 function, we generated 13xMyc-tagged variants of Oma1 wherein Cys^{272}, Cys^{332}, or both were mutated to an alanine. Although C272A substitution had no significant effect on Oma1 stability and oligomerization (Fig. 2C, D, lane 3), steady-state levels of the Oma1 C332A mutant were essentially nondetectable relative to controls (Fig. 2C, lane 4). Strikingly, the double C332A C272A mutant was expressed at normal levels (Fig. 2C, lane 5); however, the high-mass Oma1 C332A C272A complex was more labile under BN-PAGE conditions (Fig. 2D, compare lanes 2, 3, and 5). Further, both C272A and C332A C272A Oma1 oligomers were destabilized by BN-PAGE, reflecting a comparable degree of stress activation in H_2O_2-treated cells (Fig. 2E). These mutations did not affect topological properties of Oma1 (Supplementary Fig. S2). We next assessed the redox state of the mutants in question. We found that the C332A C272A Oma1 mutant was not modified by $mm(PEG)_{24}$ on pretreatment with TCEP, and the C272A Oma1 mutant displayed only partial modification after such treatment (Fig. 2F). These results demonstrate that the IMS-facing residues Cys^{272} and Cys^{332} are key contributors to the oxidized state of Oma1 and form disulfide bonds that are critical for stability of the protein. These data are also consistent with the idea that the redox status of these residues is dispensable for stress-activation of Oma1 (Figs. 1D and 2E).

Being intrigued with the drastic instability of the C332A Oma1 mutant, we wanted to investigate its fate. We first conducted quantitative real-time polymerase chain reaction (qRT-PCR) analysis of *OMA1* mRNA levels in wild type (WT) cells or *oma1*Δ cells expressing WT, C272A, or C332A variants of the protease. The levels of the *oma1 C332A* transcript were virtually indistinguishable from other *OMA1* variants (Fig. 3A), reflecting normal expression of this mutant. This result indicates that stability of the mutant is affected at a post-translational level and suggests two likely scenarios of how the C332A Oma1 mutant could be degraded: (i) The mutant is eliminated by the ubiquitin-proteasome system (UPS) while *en route* to mitochondria, or

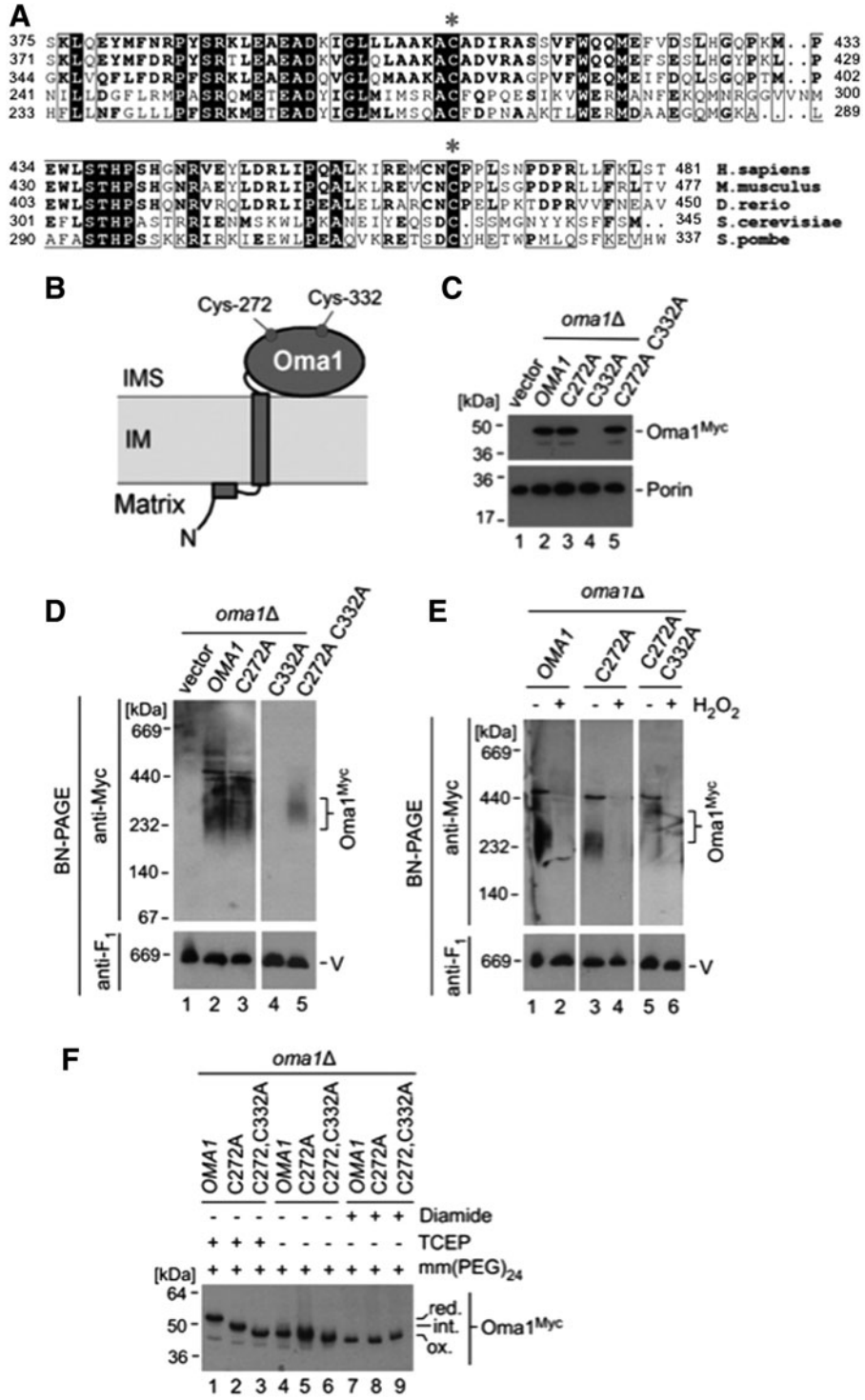

FIG. 2. Conserved IMS-facing cysteine residues mediate the semi-oxidized state and stability of Oma1. **(A)** Amino acid sequence alignment of the C-terminal portions of Oma1 from various species by using MultAlin (13) and ESPript3 (38) programs. Identical amino acid residues are shaded in *black*; the *boxes* highlight conserved and similar residues. Cys^{272} and Cys^{332} rare marked by *asterisks*. **(B)** A schematic depicting topological features of Oma1. Two conserved, IMS-facing cysteine residues, Cys^{272} and Cys^{332}, are highlighted. **(C)** Western blot analysis of mitochondria (15 μg) from *oma1*Δ cells expressing indicated variants of Oma1-13xMyc. The mitochondrial protein porin was visualized with the respective antibody and served as a loading control. **(D)** BN-PAGE analysis of mitochondria (70 μg) from **(B)** was conducted as described in Figure 1A. **(E)** Seventy micrograms of mitochondria isolated from indicated cells challenged with 1 m*M* H_2O_2 as in Figure 1A were analyzed by blue native gel electrophoresis. **(F)** Mitochondrial proteins from cells described in **(B)** were precipitated with TCA and incubated with $mm(PEG)_{24}$, TCEP, or diamide as indicated. Samples were then subjected to SDS-PAGE and analyzed by immunoblotting with anti-Myc antibody. IMS, intermembrane space.

(ii) the mutant is transported into mitochondria, but is rapidly degraded by IM protease(s). To test these scenarios, we monitored degradation of WT and C332A Oma1 variants after the inhibition of new protein synthesis by the cytosolic translation-blocking drug cycloheximide, with or without adding the UPS-specific inhibitor MG132. Although MG132 treatment slightly increased steady-state levels of the WT Oma1, we found no appreciable stabilization of the C332A mutant on UPS inhibition (Fig. 1B). This result indicates that UPS is unlikely to be involved in degradation of the C332A Oma1 mutant. Next, we assessed stability of the C332A Oma1 protein expressed in cells lacking Oma1 in combination with the loss of other IM-associated proteases: rhomboid protease Pcp1, the i-AAA protease (Yme1), the m-AAA protease (inactivated *via* deletion of its Yta10 subunit), and Atp23 metallopeptidase. Again, lack of these proteases did not result in stabilization of the C332A Oma1 mutant (Fig. 3C). Similarly, we were unable to stabilize this mutant by pretreating the cells

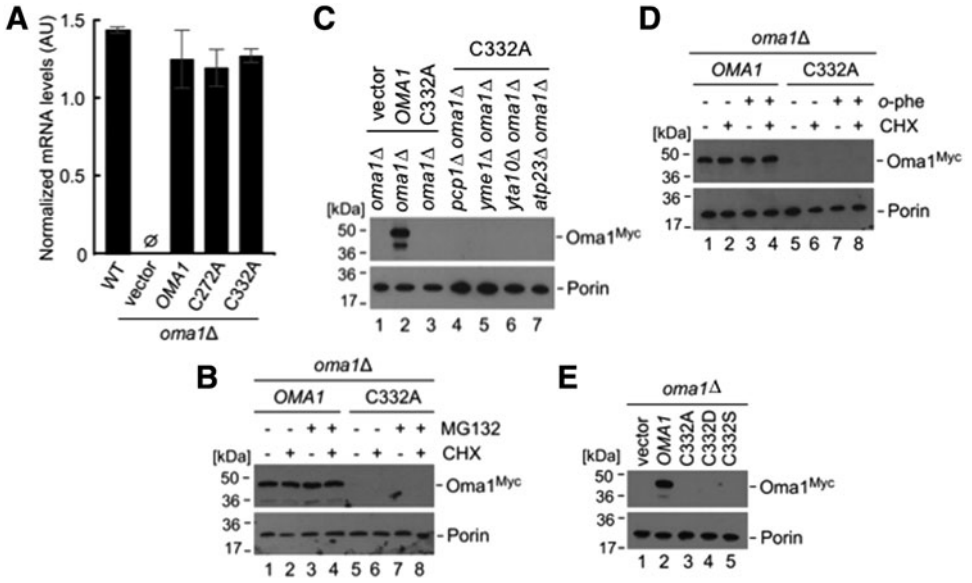

FIG. 3. Cys^{332} is an invariant residue that is crucial for Oma1 stability. (A) Transcript levels of indicated *OMA1-13xMyc* variants on their expression in *oma1*Δ cells. The data are shown as mean values ± SD ($n = 3$ biological replicates). **(B)** *oma1*Δ cells expressing WT or C332A Oma1 were first incubated in the presence of 0.01% SDS for 3 h, and then for 30 min with 200 μg/mL cycloheximide drug to stall cytosolic translation. Aftr the incubation, cells were treated with the proteasome-specific inhibitor MG132 (75 μM) for 1 h. Total cell extracts from the respective cultures were analyzed by SDS-PAGE, and antibodies against the Myc epitope were used to visualize 13xMyc-tagged Oma1. Antibodies against mitochondrial outer membrane protein porin were used to confirm equal loading. **(C)** Mitochondria isolated from indicated strains expressing C-terminally Myc-tagged WT or C332A Oma1 were subjected to SDS-PAGE and analyzed by Western blot with antibodies against the Myc epitope. Steady-state levels of the mitochondrial protein porin served as a loading control and were visualized by immunoblotting with anti-Por1 antibody. **(D)** *oma1*Δ cells expressing WT or C332A Oma1 were treated and analyzed as in **(B)** except that in this case they were treated with 2.5 mM zinc-specific chelator o-phe for 1 h to nonselectively inhibit cellular metalloproteases. **(E)** Mitochondrial lysates from cells expressing indicated Oma1 variants were analyzed by Western blotting with anti-Myc and anti-porin antibodies as in **(B)**. AU, arbitrary units; o-phe, ortho-phenanthroline; WT, wild type.

with known nonselective inhibitors of mitochondrial proteases such as ortho-phenanthroline, ethylenediaminetetraacetic acid (EDTA; to inhibit metallopeptidases), apyrase (to inhibit ATP-dependent proteases), and iodoacetamide (to inhibit cysteine proteases) (Fig. 3D and Supplementary Fig. S3A, B). We conclude that the C332A mutant form of Oma1 may be degraded either by an unidentified mitochondrial protease or through a cooperative action of several mitochondrial quality control proteases. Future studies will attempt to address this intriguing issue.

Finally, we probed the specificity of the Cys^{332} substitution for the stability of Oma1. To this end, two variant mutations were introduced into Oma1 by site-directed mutagenesis: (i) the sulfenylation-mimicking C332D mutation and (ii) the C332S mutation to test the role of the sulfhydryl side chain of Cys^{332}. None of these substitutions at Cys^{332} resulted in a stable form of Oma1 (Fig. 3E). These findings suggest a crucial role for the cysteine residue at position 332, most likely through its ability to form a disulfide bond with the Cys^{272}. Although the lack of structural data did not allow us to unequivocally determine the nature of this bond (intra- *vs.* intermolecular), the inability to stabilize the Cys^{332} mutant variants of Oma1 *in trans* (Supplementary Fig. S3C) supports the former scenario.

Disulfide bond-breaking mutations in Cys^{272} and Cys^{332} alter conformational state of Oma1

Having determined that disulfide bond-forming Cys^{272} and Cys^{332} residues are necessary for Oma1 oligomerization and stability, we next wondered whether loss of a disulfide bond in the C332A C272A Oma1 mutant could influence the conformational state of the protease. This idea is in line with our observation that in unstressed cells the double cysteine mutant Oma1 complex appears to be less stable than the WT Oma1 oligomer under native gel electrophoresis conditions (Fig. 2C). To test this hypothesis, we conducted a previously developed two-step experiment (7) outlined in Figure 4A. First, we isolated mitochondria from either unperturbed or CCCP-treated cells expressing 13xMyc-tagged WT or C332A C272A Oma1 variants. The respective mitochondrial lysates were then subjected to high-velocity sucrose gradient fractionation of the complex in question. Consistent with our previous finding that conformation-altered Oma1 oligomers are not destabilized by the mild (relative to BN-PAGE) conditions of sucrose gradient fractionation (7), we observed no significant differences in the migration pattern of the variant Oma1 high-mass complexes (Fig. 4B). Next, we isolated Oma1 complex-containing fractions and evaluated their resistance toward low amounts of externally added proteinase K. As predicted from the model wherein conformationally altered Oma1 oligomers exhibit increased susceptibility to proteinase K, we found that the C332A C272A Oma1 oligomers from unstressed cells exhibited markedly increased sensitivity to limited proteolysis by this enzyme compared with WT Oma1 complexes (Fig. 4C and Supplementary Fig. S4).

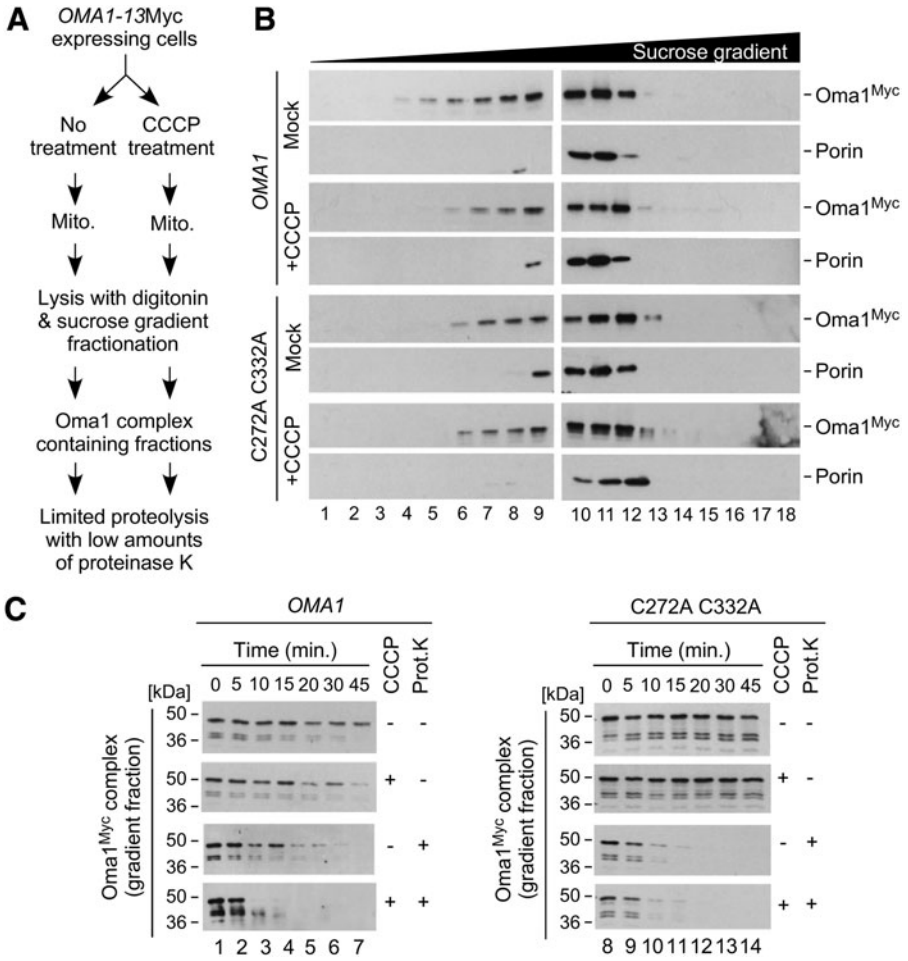

FIG. 4. Disulfide bond formed by Cys^{272} and Cys^{332} influences conformation state of Oma1. (A) A schematic outlining the design of experiments to probe for conformational changes in the Oma1 oligomeric complex. *oma1*Δ cells expressing C-terminally 13xMyc epitope-tagged WT or C332A C272A Oma1 were challenged with 45 μM CCCP for 2 h or left untreated. Seven hundred micrograms of mitochondria from the respective cells were lysed in a buffer containing 1% digitonin and subjected to sucrose density gradient (10–50%) ultra-fractionation to isolate high-mass fractions containing Oma1-13xMyc protein complexes. Isolated fractions (10–12) were pooled together and incubated with or without low amounts of proteinase K (Prot. K; 0.4 μg/mL) for up to 45 min on ice. Aliquots were collected at the times indicated in **(C)** and analyzed by immunoblotting with anti-Myc antibody. **(B)** Representative blots of velocity gradient-fractionated Oma1-13xMyc complexes from mitochondria of the WT or C332A C272A Oma1-expressing cells that were stressed with CCCP or left untreated. Collected fractions were analyzed by using anti-Myc to detect Oma1 oligomers and anti-porin to visualize the 440 kDa porin complex for size comparison. Note that abundance/stability of the C332A C272A Oma1 oligomeric species is unaffected by gradient fractionation conditions relative to WT Oma1 complex. **(C)** Western blot analysis of relevant Oma1-13xMyc high mass-complex-containing fractions isolated in **(B)** and treated with or without minute amounts of proteinase K for indicated periods.

Consistently with unaltered steady-state levels of the C332A C272A Oma1 mutant, the stability of the respective gradient fractions that did not receive proteinase K treatment was comparable to that of WT Oma1. Finally, in line with our finding that both the WT and double cysteine mutant Oma1 complexes are destabilized on stress-activation (Fig. 2E), we observed no significant differences in their susceptibility to proteinase K between the oligomeric Oma1 species derived from CCCP-treated cells. Together with the observed destabilizing effect of the C332A mutation, these results support the model that the disulfide bond formed by Cys^{272} and Cys^{332} likely plays a structural role and mediates conformational stability of the Oma1 high-mass complex.

Oma1 complex is dynamically tuned in a redox-sensitive manner

To test the hypothesis that the Oma1 complex can be dynamically influenced by changes in its oxidation state, we employed an *in vitro* assay wherein we used BN-PAGE to monitor stability of the activated WT and C332A C272A Oma1 oligomers subjected to a postisolation reduction. In this assay, mitochondria isolated from CCCP-treated *oma1*Δ cells expressing relevant Oma1 variants were treated with thiol (DTT) or nonthiol (sodium ascorbate) reducing agents and analyzed by BN-PAGE. In these assays, pretreatment with dithiothreitol (DTT) but not ascorbate led to marked stabilization of the activated WT Oma1 oligomer relative to

controls (Fig. 5A, compare lanes 2 and 3). In contrast, pretreatment with DTT had no appreciable stabilizing effect on the complex derived from CCCP-stressed *oma1*Δ cells expressing the C332A C272A Oma1 mutant. These data validate our prediction that thiol-mediated reduction of Cys^{272} and Cys^{332} leads to conformational stabilization of the Oma1 oligomer and further suggest that these residues may also be playing a role in the redox-tuning of Oma1.

To further test this idea, we examined *in vitro* proteolytic activity of Oma1 in the presence of increasing amounts of reducing agent, using a previously developed fluorescein isothiocyanate (FITC) casein processing assay (7, 24). To this end, we isolated mitochondrial membranes from Oma1- and C332A C272A Oma1-expressing *oma1*Δ cells treated with CCCP to activate the protease. We then incubated ATP-deprived membranes with FITC-casein in the presence of 0–10 m*M* DTT or 0–5 m*M* sodium ascorbate and monitored changes in FITC fluorescence, which reflects proteolytic conversion of the substrate. The rate of FITC fluorescence generated by either Oma1 variant declined with increasing concentrations of DTT, indicating inhibition of Oma1 proteolytic activity (Fig. 5B). Strikingly, however, sensitivity of Oma1 toward reductant was markedly diminished in the case of the C332A C272A Oma1 mutant, demonstrating that Cys^{272} and Cys^{332} are important for redox modulation of the enzyme (Fig. 5B). In contrast, we found no significant changes in the efficiency of FITC-casein proteolysis when the samples were preincubated with sodium ascorbate (Fig. 5C). In all cases, the steady-state levels of each Oma1 variant were not significantly influenced (Fig. 5D). These results indicate that changes in the redox state of mitochondria may regulate Oma1 stability and activity *via* Cys^{272} and Cys^{332}.

Next, we wanted to corroborate our findings *in vivo*. Because the redox environment of the IMS is quite unique and cannot be easily genetically modified (9, 26), we decided to focus instead on a downstream condition wherein cells are impaired in their ability to efficiently generate disulfide bonds in the IMS. To this end, we evaluated the biochemical behavior of WT and C332A C272A Oma1 variants in the *mia40-4* genetic background. This temperature-sensitive allele of the mitochondrial oxidoreductase Mia40 produces a substrate release-impaired enzyme, thereby affecting cysteine oxidation in the IMS (10). Consistent with the essential role of Mia40 in disulfide formation in the IMS, glucose growth of both *mia40-4* and *oma1*Δ *mia40-4* strains was severely impaired when cells were cultured at a nonpermissive temperature (Fig. 6A). We isolated mitochondria from *oma1*Δ *mia40-4* cells expressing WT or C332A C272A Oma1 cultured at

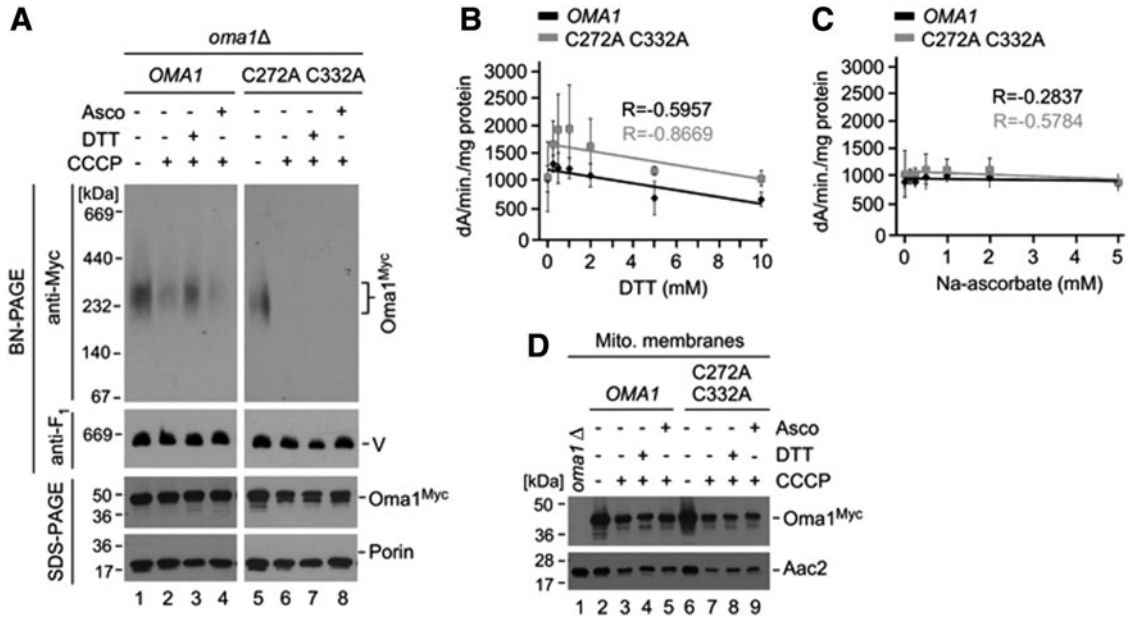

FIG. 5. Oligomerization and activity of Oma1 are tuned in a redox-dependent manner. (A) BN-PAGE and SDS-PAGE analysis of mitochondria isolated from *oma1*Δ cells expressing WT or C332A C272A Oma1 treated with or without CCCP (45 μM for 2 h). After the isolation and lysis with digitonin, mitochondrial extracts were incubated with 10 m*M* DTT or 5 m*M* sodium ascorbate for 45 min on ice, or left untreated. The samples were then subjected to native or denaturing gel electrophoresis. Immunoblotting procedures to visualize indicated proteins or protein complexes were carried out as described in Figure 1A and B. **(B, C)** ATP-independent proteolytic activity of mitochondrial membranes derived from CCCP-treated *oma1*Δ cells expressing WT or C332A C272A Oma1 in the presence of indicated concentrations of DTT **(B)** and sodium ascorbate **(C)**. Ten micrograms of ATP-depleted membrane fractions derived from relevant isolated mitochondria were resuspended in the reaction buffer containing indicated amounts of the reducing agents and incubated at room temperature for 5 min. After that, samples were supplemented with 5 μM FITC-casein fluorogenic substrate and incubated at 25°C for 35 min. After incubation, membranes were sedimented by centrifugation; supernatant fractions were collected and used in subsequent fluorescence measurements. Normalized fluorescence intensities were measured as described in the Materials and Methods section at 485-nm excitation and 528-nm emission wavelengths. The error bars indicate SD ($n=4$ biological replicates). *R* values were calculated by using Microsoft Excel. **(D)** Steady-state levels of Oma1-13xMyc variants with loading control inner membrane carrier protein Aac2, in mitochondrial membranes isolated from samples described in **(A)** were analyzed by Western blot with respective antibodies. DTT, dithiothreitol; FITC, fluorescein isothiocyanate.

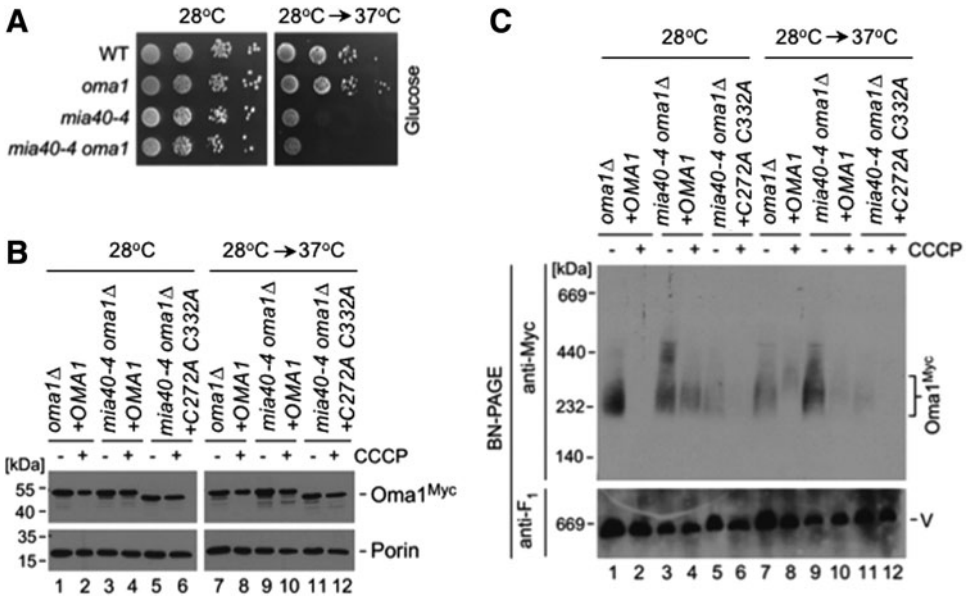

FIG. 6. ***In vivo*** **redox-tuning of Oma1. (A)** Glucose growth test of WT, *oma1*Δ, *mia40-4*, and *oma1*Δ *mia40-4* strains. Cells were precultured at 28°C in 2% glucose-containing YPD medium and then split into two cultures, one of which was further cultured at 28°C whereas the other one was incubated at 37°C for 12 h (labeled as 28°C/37°C) to stimulate the temperature-sensitive phenotype in the strains bearing *mia40-4* allele. After incubation, serial dilutions of the cells were dropped onto solid YPD medium and incubated at 28°C and 37°C. Pictures were taken after 2 days of incubation. **(B)** Steady-state levels of Oma1-13xMyc variants with loading control (porin) in mitochondria isolated from indicated transformant cells that were cultured at 28°C or 28°C/37°C conditions and with or without additional stress challenge with CCCP (45 μM for 2 h). Samples were analyzed by SDS-PAGE immunoblotting as in Figure 3C. **(C)** BN-PAGE analysis of mitochondrial lysates from samples described in **(B)**. Oma1-13xMyc complexes were visualized by blotting for Myc-epitope, and respiratory complex V (loading control) was detected by using anti-F_1 serum.

normal or restrictive temperatures and with or without addition of CCCP. In all cases tested, steady-state levels of either Oma1 variant were unchanged when compared with relevant controls (Fig. 6B). We next assessed the stability of the Oma1 oligomers by BN-PAGE. Although temperature inactivation of Mia40 had no appreciable stabilization effect on the Oma1 oligomer in CCCP-treated cells—likely due to insufficiently compromised redox equilibrium—we found that stability of the Oma1 complex was strongly increased in *mia40-4* cells cultured at 37°C relative to controls (Fig. 6C, compare lanes 3, 7, and 9). In contrast, Mia40 inactivation had no stabilizing effect on the C332A C272A Oma1 complex (Fig. 6C, compare lanes 5 and 11), further supporting the notion that stability and/or activity of Oma1 may be influenced by Mia40 through Cys^{272} and Cys^{332} residues of the protease.

Oma1 interacts with its engineered substrate in a redox-dependent manner

We wanted to further refine our understanding of how changes in Oma1 oxidation state might influence the protease's interaction with its substrates. One caveat is that the known repertoire of Oma1 substrates in yeast is limited to proteins that cannot be easily studied due to their large size, hydrophobicity, or mitochondrial genome origin. We, therefore, designed a chimeric protein—designated S1-1–consisting of the 1–104 N-terminal residues of cytochrome *c* oxidase assembly factor Sco2 (comprising the mitochondrial targeting signal and a transmembrane helix motif) and a 225–244 residue segment derived from the Oma1 substrate protein Oxa1 L240S that harbors an experimentally identified Oma1 cleavage site (22), followed by a 159–250 residue globular domain of cytosolic monothiol glutaredoxin 3, and finally a FLAG epitope tag (Fig. 7A). To minimize any interference from Grx3s cysteine residue on IMS or Oma1 redox balance, its potentially redox-active Cys^{176} residue was mutated to an alanine. For our subsequent analyses, we co-expressed S1-1 along with the 13xMyc-tagged Oma1 in *oma1*Δ cells (Supplementary Fig. S5). S1-1 expression yielded a protein of about 36 kDa as well as a ~17 kDa cleavage product matching the predicted size of the chimera's IMS-exposed moiety, which was not produced in the absence of Oma1 (Fig. 7B). S1-1 was successfully targeted to mitochondria and inserted into the IM, as indicated by its resistance to alkaline carbonate extraction similar to that of IM-anchored protein Cox2 (Fig. 7C). Proteinase K protection experiments further confirmed that S1-1 acquired proper topological orientation in the IM with its C-terminal portion facing the IMS, as reflected by its sensitivity to exogenously added proteinase K in osmotically compromised (swollen) mitochondria (Fig. 7D).

Having confirmed that S1-1 is appropriately targeted and positioned in the IM, we asked whether it could trigger Oma1 activation. To this end, we monitored stability of the Oma1 oligomeric complex in mitochondria from cells expressing S1-1 by BN-PAGE. We found that S1-1 expression resulted in enhanced lability of the Oma1 oligomer relative to untransformed control and was comparable to that observed in CCCP-treated cells (Fig. 7E). As predicted, the steady-state levels of Oma1 remained unchanged at all conditions tested. To further confirm Oma1 activation by S1-1, we examined

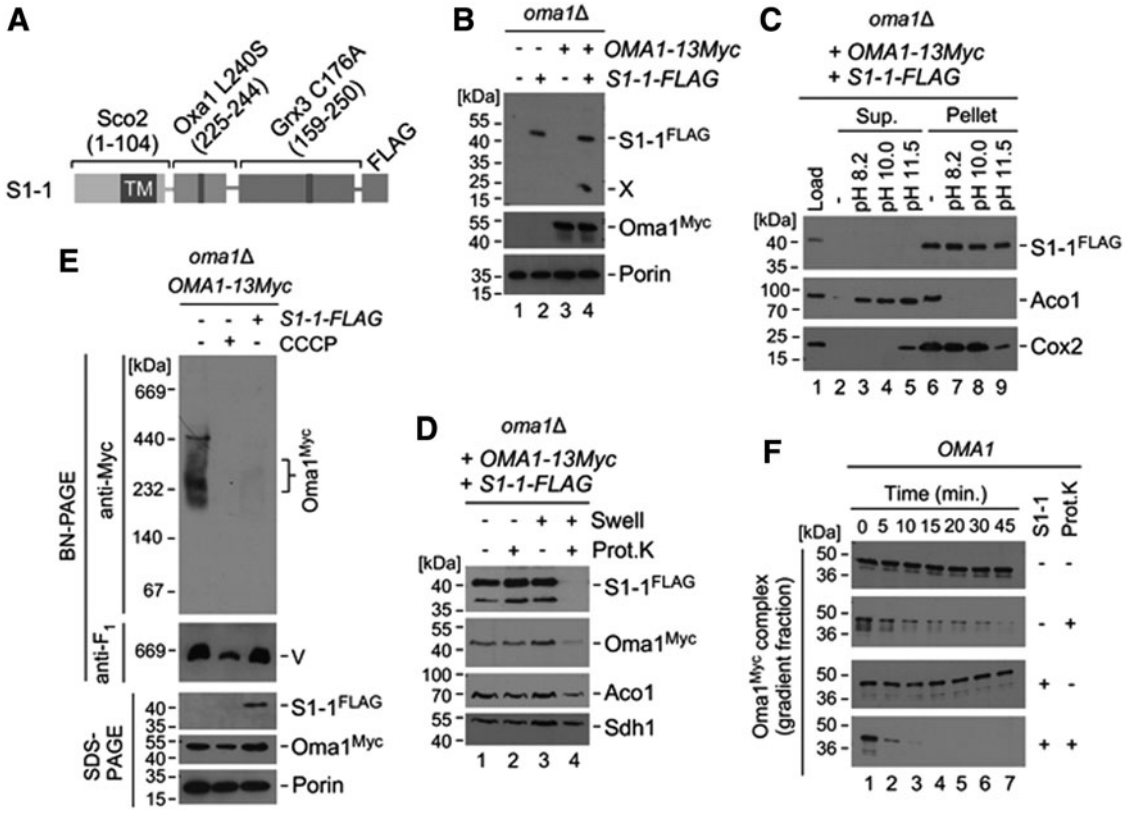

FIG. 7. Engineering of S1-1 artificial Oma1 substrate. (A) Schematic depiction of S1-1 chimeric protein encompassing the N-terminal portion of cytochrome *c* oxidase assembly factor Sco2 (residues 1–104; original protein numbering), a segment derived from the L240S mutant of IM insertase Oxa1 (residues 225–244) and the globular domain of cytosolic glutaredoxin 3 (Grx3, residues 159–250) followed by the C-terminal FLAG-epitope tag. Note that the potentially reactive Cys^{176} residue of Grx3 was mutated to an alanine to avoid any potential redox-based engagement of the protein with Oma1. **(B)** Expression of S1-1-FLAG with or without Oma1-13xMyc in *oma1*Δ cells was analyzed by immunoblotting with anti-FLAG and anti-Myc antibodies, and anti-porin antibody was used as a loading control. X denotes S1-1 cleavage product. **(C)** Mitochondria isolated from cells described earlier were used to analyze membrane association of S1-1 with mitochondrial membranes. Purified organelles were treated with 0.1 *M* sodium bicarbonate at indicated alkaline conditions for 1 h on ice. After the treatment, mitochondria were fractionated to separate soluble and integral membrane proteins. Samples were subjected to SDS-PAGE immunoblot analysis by using anti-FLAG antibody to detect S1-1, antibodies against cytochrome *c* oxidase complex subunit Cox2, and antisera against the metabolic enzyme aconitase (Aco1), which served as markers of integral membrane association and soluble protein, respectively. **(D)** Sub-mitochondrial compartmentalization of S1-1 was determined by using the S1-1-FLAG harboring mitochondria described in **(B)**. Purified mitochondria were incubated with the exogenously added proteinase K (Prot. K 1 μg/mL) for 30 min on ice after either no treatment or hypotonic swelling (Swell) to fragment the outer mitochondrial membrane. Subsequently, the samples were analyzed by SDS-PAGE immunoblotting using anti-FLAG and anti-Myc antibodies to visualize S1-1 and Oma1, respectively. Mitochondrial matrix proteins Sdh1 and aconitase served as markers for sub-mitochondrial localization and were visualized by using anti-Sdh1 and anti-Aco1, respectively. **(E)** BN-PAGE and SDS-PAGE analysis of the Oma1 complex in mitochondria from **(B)** or *oma1*Δ cells expressing Oma1-13xMyc and treated with CCCP as in Figure 5A was conducted as described in Figure 1A. **(F)** Oma1 complex-enriched sucrose gradient fractions from mitochondrial lysates of *oma1*Δ strain expressing Oma1-13xMyc with or without S1-1-FLAG were isolated and assayed for conformational changes by using low amounts of proteinase K as in Figure 4. IM, inner mitochondrial membrane.

sensitivity of sucrose gradient-isolated Oma1 oligomers to low amounts of exogenously added proteinase K. Consistent with our earlier observations, expression of S1-1 significantly increased sensitivity of the Oma1 oligomers to limited proteolysis relative to control, thereby reflecting changes in conformation/stability of the complex on S1-1 expression (Fig. 7F). Altogether, these results strongly suggest that S1-1 is a substrate that, indeed, can effectively activate Oma1.

Next, we wanted to determine whether Oma1 can bind to S1-1 and whether this binding could be influenced by changes in redox state of the protease. To address these questions, we conducted co-immunoprecipitations (coIPs) of Oma1 with the S1-1 chimera in mitochondrial lysates from normal and CCCP-stressed cells, in the presence or absence of 10 m*M* DTT. As predicted, our coIP studies showed a clear interaction of Oma1 with S1-1 in normal and—although slightly less robustly—CCCP-challenged cells (Fig. 8). Strikingly, this interaction was effectively abrogated on addition of DTT (Fig. 8, lanes 7–10). These results demonstrate that Oma1 interacts with S1-1 in a redox-sensitive manner. More generally, these data suggest that redox modification of Oma1 might be influencing its ability to interact with its natural substrates. Future studies are warranted to further investigate this exciting question.

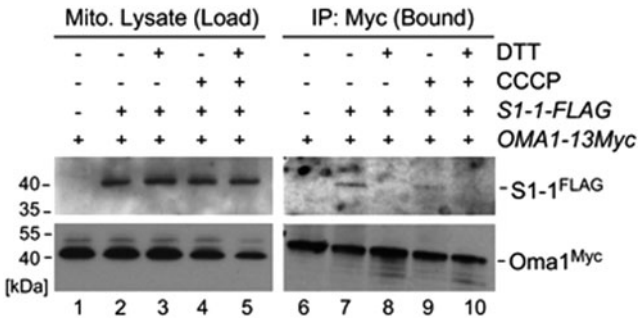

FIG. 8. Oma1 binds to S1-1 substrate in a redox-sensitive manner. Digitonin-solubilized mitochondrial lysates (500 μg) from *oma1*Δ cells expressing Oma1-13xMyc with or without S1-1-FLAG and stressed or not with CCCP as in Figure 5A were incubated with anti-Myc magnetic beads for 24 h at 4°C. Incubations were conducted in the presence or absence of 10 m*M* DTT. After extensive washes, immunoadsorbed proteins (bound fraction; 50% loaded) were subjected to SDS-PAGE/Western blot analysis with indicated antibodies, along with the mitochondrial lysates before incubation (load fraction; 5% loaded).

Discussion

The sheer complexity of the IM sub-proteome and inherent risk of generation of byproduct superoxide radicals by mitochondrial respiratory chain enzymes creates a challenging proteostatic environment with a high probability of protein malfunction. This, in turn, can further impair IM permeability, ion homeostasis, and ATP production, ultimately leading to cell demise (29). Unsurprisingly, these conditions are now recognized as a root cause of a wide variety of prevalent human pathologies, including cardiovascular and neurodegenerative diseases (29, 33). A network of mitochondrial quality control mechanisms is in place to avert these scenarios and maintain normal mitochondrial functions. The stress-activated metallopeptidase Oma1 operates on the IMS side of the IM, has emerged as a potential molecular nexus for several quality control activities (3, 28), and is a prospective therapeutic target in mitochondria (1, 27, 39). In spite of its importance, only limited structural and molecular data on Oma1 are available, which offer very little insight into its function. As such, it is important to elucidate molecular details of Oma1 function in the context of the dynamic redox environment of the IMS.

In this work, we sought to better understand how Oma1 activity is regulated and adjusted in response to various physiological demands. Using the yeast model, we discovered that Oma1 shares features of a *bona fide* redox-dependent protein and determined that the protease exists in a semi-oxidized state under both normal and stressed conditions. Importantly, we also found that the human ortholog of Oma1 shares these biochemical properties, thereby underscoring the evolutionary conservation of this biochemical trait. Interestingly, the oxidation state of the protease was largely unaltered on stress-activation by acute cellular insults with H_2O_2 or the uncoupler CCCP. These results suggest two possible scenarios: (i) Changes in the redox status of Oma1 may not be sufficient to trigger its activation in response to these stimuli, or (ii) these stressors may be causing drastic changes in the IMS environment wherein a delicate redox-tuning may not be an optimal regulatory response. Consistent with the first idea is our finding that acutely challenging cells with 100 m*M* DTT had no effect on Oma1 activation (data not shown). On the other hand, our *in vitro* functional analyses indicated that increased thiol reduction of Oma1 may reduce its proteolytic activity concomitant with stabilization of the Oma1 oligomeric complex. These data are in line with a previously observed inverse correlation between Oma1 complex activity and proteolytic activity of the enzyme (7). Our experiments in *mia40-4* background that aimed at examining Oma1 behavior under a condition wherein normal disulfide bond formation in the IMS is impeded indicate that the oxidation state of the protease correlates with its stability. It is noteworthy that *in vivo* the IMS redox environment appears to be better buffered by reduced glutathione that can freely diffuse from the cytosol (9, 26), which could potentially explain the only modest stabilizing effect observed in the *mia40-4* mutant.

These results also raise an interesting possibility that Mia40 may be involved in the redox-tuning of the Oma1 complex, in a manner reminiscent of that reported for the Atp23 protease (40) and the Mic19 subunit of the MICOS (mitochondrial contact site and cristae organizing system) machinery (38). How might Oma1 be activated when redox changes can be excluded? Our data suggest that additional molecular features of the protease could be important for conformational rearrangements required for Oma1 stress-activation. This notion is consistent with previous reports showing Oma1 activation in certain mutants or on conditions that do not appear to elicit any significant changes in mitochondrial redox homeostasis (4, 5, 24). Fundamental understanding of these molecular features and events is limited due to complete lack of structural data on Oma1. It is possible, however, that changes in the redox status of Oma1 might influence the enzyme's activation, as discussed later.

Some mechanistic insights into molecular determinants of Oma1 stabilization also emerged from this study. Our analyses identified the conserved IMS-exposed Cys^{332} and Cys^{272} residues of Oma1 as key contributors to the protease's oxidized state. The nearly invariant nature of the C-terminal Cys^{332} points at its involvement in a structural, most likely intramolecular, disulfide bond. Such molecular architecture is reminiscent of an intramolecular disulfide bond in the enterobacterial Lon protease (31), which has been proposed to function as a switch to optimize Lon's proteolytic activity depending on the redox environment. The stabilizing effect of the C272A mutation in the C332A backbone is remarkable and implicates Cys^{272} as a second residue involved in the bond. Notably, the C332A C272A Oma1 mutant was shown to be less stable than the WT protease, thereby suggesting a structural role for the Cys^{272}-Cys^{332} bond in conformational stability of the Oma1 high-mass complex. Of note, in our earlier study (7), we were able to observe a partially stabilized C332A mutant, likely because of the miniature His-Myc epitope tag that was used to visualize steady-state levels of the mutant protein, as opposed to the much larger 13xMyc tag used in this study. It is, thus, possible that the latter tag further affects the already compromised stability of the Cys^{272}-Cys^{332} bond-deprived protein.

Despite extensive efforts, we were unable to identify factors responsible for rapid post-translational degradation of the C332A Oma1 mutant. Two potential explanations for such a fate are envisioned. First, degradation of the C322A Oma1 mutant may occur through a concerted action of several

mitochondrial proteases, and inhibition or removal of one proteolytic component may not significantly impair its proteolysis. Indeed, similar degradation mechanisms have been suggested for mutant forms of the IM insertase, Oxa1 (22), and mitochondrial phosphatidylserine decarboxylase Psd1 (32). A second, less likely, scenario considers the possibility that the C322A Oma1 mutant could be degraded by an unidentified mitochondrial protease that eluded our prediction-based analyses.

Finally, we engineered an S1-1 chimeric protein that can efficiently activate Oma1 when targeted to mitochondria. S1-1 readily binds to Oma1 regardless of its activation state, thus indicating that the 19-residue segment derived from L240S Oxa1 mutant is sufficient to mediate S1-1 recognition and cleavage by the protease. These data also suggest the relative promiscuity of Oma1 toward its substrates. Importantly, we found that Oma1 interacts with S1-1 in a redox-sensitive manner, wherein S1-1 binding to Oma1 is effectively abrogated in the presence of DTT. As S1-1 is designed in such a way that it contains no cysteine residues, the sensitivity of Oma1-S1-1 interaction is unlikely to arise from the disruption of intermolecular disulfide bonding between the two proteins. Taken together, our results suggest that redox modifications of the Cys^{272}-Cys^{332} bond might be influencing the enzyme's ability to either interact or maintain an association with its natural substrates. It is also tempting to speculate that this disulfide bond might be dynamically influenced by additional cysteine-rich proteins in the IMS such as Atp23 *via* reversible formation of intermolecular mixed disulfides. Our study establishes the framework for further structural studies directed at resolving molecular determinants for substrate recognition and redox-tuning of Oma1. Given the central role of Oma1 in mitochondrial function and integrity, this study opens an exciting research avenue regarding how changes to the cellular and mitochondrial redox environment might be influencing the proteolytic control of these processes in normal and pathological states.

Materials and Methods

Yeast strains, plasmids, and growth conditions

Yeast strains used in this work are listed in Supplementary Table S1. Yeast cells were cultured in rich YPD (1% yeast extract, 2% peptone, and 2% glucose), or complete synthetic medium supplemented with relevant amino acids and containing 2% glucose or 2% glycerol/2% D-lactic acid mix as a carbon source. *OMA1* containing C-terminal 13xMyc was expressed from pRS425 vector under control of the native promoter and *ADH1* terminator (7); or a 1xFLAG epitope tagged version was inserted into pRS426 vector under control of the *MET25* promoter and *CYC1* terminator. The C272A, C332A, C332D, C332S, and C332A C272A mutant variants of Oma1 were generated by site-directed mutagenesis using the Phusion kit (Thermo Fisher Scientific). Yeast deletion strains were constructed by using pAG60 plasmid-derived deletion cassettes as previously described (7). To generate a plasmid expressing S1-1 chimeric protein, the N-terminal portion of Sco2 (amino acid residues 1–104) with a flanking region containing a 19-residue segment (VDGFANQGVAWFTDSTQAD), corresponding to the L240S mutant of the IM insertase Oxa1 reported to harbor the Oma1 cleavage site (22), were PCR amplified from genomic DNA of the respective strain (22), using primers Sco2-For and Sco2-Oxa1-Rev (Supplementary Table S2). In a separate set of reactions, the C-terminal fragment of glutaredoxin Grx3 (amino acid residues 159–250) with flanking regions containing sequences homologous to the Oxa1 L240S segment at the 5′-end and the 3′-end FLAG epitope tag was PCR amplified from yeast genomic DNA by using primers Oxa1ts-Grx3-For and Grx3-FLAG-Rev. In the next round, gel-purified products of the reactions described earlier were joined together by overlap extension PCR using primers Sco2-For-Short and Grx3-FLAG-Rev-Short bearing 5′-*Sac*I and 3′-*Xho*I restriction sites, respectively. The obtained product was cloned into the pRS423 expression vector under the control of the *MET25* and *CYC1* terminator. Finally, the C176A mutation was introduced by site-directed mutagenesis. The constructs were confirmed by DNA sequencing.

The ability of strains to utilize various carbon sources was tested by spotting serial dilutions of the cells onto complete synthetic plates containing 2% glucose or 2% glycerol and 2% D-lactic acid. The cells were pregrown overnight in corresponding selective media as indicated earlier. The plates were then incubated at 28°C and 37°C for 2–4 days. To test the growth of strains bearing the *mia40-4* temperature-sensitive allele, the cells were precultured in selective media for 24 h at 28°C. After the incubation, the cells were split into two cultures, one of which was left to grow at 28°C whereas the other culture was incubated at 37°C for another 12 h.

Gene expression analysis

Total mRNA was isolated from 5-mL cultures grown overnight in selective minimal medium. The cells were pelleted by quick centrifugation (5000 *g* for 1 min), washed twice with water, and immediately used for RNA isolation with yeast RNA purification kit (Epicentre) according to the manufacturer's instructions. cDNA synthesis was performed by using Maxima H Minus cDNA Synthesis Master Mix (Thermo Fisher Scientific). The qRT-PCR was carried out on a Bio-Rad iCycler by using SYBR GreenER™ qPCR SuperMix Universal (Thermo Fisher Scientific) in a 96-well plate using the following conditions: 50°C for 2 min, 95°C for 10 min, 95°C for 10 s, and 60°C for 60 s for 40 cycles. All samples were analyzed in triplicate. The mRNA levels were normalized to *ACT1* transcript levels. The parametric Student's *t*-test was used to determine significance. *p*-Values of <0.05 were considered statistically significant.

Alkaline lysis of yeast cells

Whole-cell extracts were prepared according to a published protocol (24). Briefly, pelleted cells ($A_{600} = 1.0$) were resuspended in 250 μL of 50 m*M* Tris-HCl, pH 8.0, followed by addition of 50 μL of the lysis buffer containing 10 *M* NaOH, 7.5% β-mercaptoethanol, and 2 m*M* phenylmethylsulfonyl fluoride (PMSF). The samples were mixed vigorously and incubated on ice for 15 min, and after addition of 220 μL of cold 100% trichloroacetic acid (TCA), they were incubated for another 15 min on ice. The samples were then precipitated by centrifugation at 20,000 *g* for 10 min at 4°C. The resulting pellets were washed twice with 1 mL of absolute acetone, air-dried on ice, and resuspended in 133 μL of 1 × Laemmli buffer followed by incubation at 85°C for 10 min. Twenty microliters of obtained samples were then used for sodium dodecyl

sulfate–polyacrylamide gel electrophoresis (SDS-PAGE) analysis.

Mitochondria isolation and purification

Yeast mitochondria were isolated from 1-L cultures grown overnight in a relevant selective media essentially as described (15) Cells were collected by centrifugation at 3500 *g* for 5 min and washed once with water. The pellets were then resuspended in 0.1 *M* Tris-SO_4, pH 9.4 (buffer A) with 10 m*M* DTT according to the ratio of 1 mL of the buffer per 0.5 g wet weight of pellets. After incubation at 30°C for 10 min, the cells were washed once with 20 mL of 1.2 *M* sorbitol (buffer C). The spheroplasts were obtained by incubation in 1.2 *M* sorbitol, 20 m*M* KH_2PO_4, pH 7.4 (1 mL of buffer B per 0.15 g wet weight) with lyticase (Sigma-Aldrich) at 4 mg/g wet weight ratio for 1 h at 30°C and gentle shaking. The samples were pelleted, washed once with 30 mL of 1.2 *M* sorbitol, and resuspended in 10 mL of 0.65 *M* sorbitol, 10 m*M* Tris-HCl, pH 7.4, 1 m*M* PMSF (buffer D). The spheroplasts were homogenized by 15 strokes in a 40-mL dounce homogenizer (Kontes Glass Co.) on ice and centrifuged at 3500 *g* for 5 min at 4°C. The supernatants were collected in separate tubes, and the pellets were homogenized two more times. Total supernatants were centrifuged at 12,000 *g* for 10 min at 4°C. The supernatants and the lipid layer on the tube walls were removed; the pellets were gently resuspended in 10 mL of buffer D and centrifuged at 2500 *g* for 5 min at 4°C. The supernatants were transferred into new tubes and precipitated by centrifugation at 12,000 *g* for 10 min at 4°C. The obtained mitochondria-enriched pellets were then resuspended in 750 μL of buffer D.

Isolated mitochondria-enriched fractions were further purified by using a discontinuous Histodenz (Sigma-Aldrich) gradient as previously described (42). Briefly, the gradient was formed by layering 10 mL of 14% (w/v) Histodenz solution in 1.2 *M* sorbitol on top of 5 mL of 22% (w/v) Histodenz soulution in 1.2 *M* sorbitol. Then, 1.5 mL of crude mitochondria were layered on top of the gradient and centrifuged at 50,000 *g* for 1.5 h at 4°C. Pure mitochondria were transferred from the interphase fraction between the two Histodenz densities into a new tube, mixed with 20 mL of buffer D, and centrifuged at 12,000 *g* for 10 min at 4°C. The pellets were gently resuspended in 1.5 mL of the same buffer, transferred into microtubes, and reisolated again. The final pellets were resuspended in 500 μL of buffer D.

Mitochondria from HEK293T human embryonic kidney cells were isolated according to Chen *et al.* (12). Total mitochondrial protein concentrations were determined by using the Coomassie Plus protein assay kit (Thermo Fisher Scientific).

Mitochondrial assays

High-velocity fractionation of protein complexes was performed in continuous 10%–50% sucrose gradient as previously described (23, 24). In brief, the gradient was formed by a gentle layering of 100 μL 80% sucrose (bottom cushion) and 2.15 mL of 50% sucrose in the stock buffer (0.1% digitonin, 20 m*M* HEPES, pH 7.4, 150 m*M* KCl, 1.2 m*M* $MgCl_2$, 0.5 m*M* PMSF), followed by 2.25 mL of 10% sucrose in the stock buffer in 5-mL tubes (Beckman-Coulter). The tubes were then set at a 45°C angle for 3 h at 4°C to allow diffusion-based equilibration. Seven hundred micrograms of mitochondria were reisolated at 12,000 *g* for 10 min at 4°C and lysed in 450 μL of lysis buffer (1% digitonin, 20 m*M* HEPES, pH 7.4, 150 m*M* KCl, 1.2 m*M* $MgCl_2$, 0.5 m*M* PMSF) for 15 min on ice. The samples were then centrifuged at 20,000 *g* for 15 min at 4°C, and clarified lysates were loaded onto the gradient and fractionated at 148,000 *g* for 6 h at 4°C. Fractions were manually collected as 250-μL aliquots, flash-frozen in liquid nitrogen, and stored at −80°C.

Sucrose fractions #10–12 were subjected to limited proteolysis by proteinase K (7). One hundred microliters of each fraction were combined together, mixed well, and split into two separate aliquots. One aliquot was treated with 1.5 μL of Proteinase K solution (40 μg/mL), and the other was used as a untreated control; all samples were kept on ice. The 15-μL aliquots were collected on addition of Proteinase K (0 min), and during the following time periods of 5, 10, 15, 20, 30, and 45 min. Collected samples were immediately mixed with 5 μL of 6 × Laemmli buffer with 5% β-mercaptoethanol and 0.8 μL of 200 m*M* PMSF, and they were incubated for 10 min at 100°C. The samples were subjected to SDS-PAGE analysis no later than 1 h after the end of the treatment.

Mitochondrial topology of the S1-1 chimeric protein was analyzed according to previously published protocols (25, 42). Six aliquots of gradient-purified mitochondria (20 μg/sample) were pelleted by centrifugation at 12,000 *g* for 10 min at 4°C and subjected to the following treatments: (i) intact mitochondria in 500 μL of 0.65 *M* Sorbitol, 10 m*M* Tris-HCl, pH 7.4; (ii) intact mitochondria in 500 μL of 0.65 *M* Sorbitol, 10 m*M* Tris-HCl, pH 7.4 with 5 μL Proteinase K (100 μg/mL); (iii) hypotonic swelling in 500 μL of 20 m*M* HEPES, pH 7.4; (iv) in 500 μL of 20 m*M* HEPES, pH 7.4 with 5 μL Proteinase K (100 μg/mL); (v) lysed mitochondria in 450 μL of 20 m*M* HEPES, pH 7.4 with 50 μL 10% DDM (n-dodecyl-β-D-Maltoside); (vi) in 450 μL of 20 m*M* HEPES, pH 7.4 with 50 μL 10% DDM and 5 μL Proteinase K (100 μg/mL). All samples were incubated on ice for 30 min with periodical mixing; then, they were treated with 55 μL of 100% w/v TCA as described earlier. The final pellets were resuspended in 50 μL of 1 × Laemmli buffer with 5% β-mercaptoethanol, incubated for 10 min at 85°C, and finally used for SDS-PAGE analysis.

Membrane association of the S1-1 chimera was determined by carbonate extraction, as described earlier (25, 42). Four aliquots of 50 μg of gradient-purified mitochondria were pelleted by centrifugation at 12,000 *g* for 10 min at 4°C. The pellets were then resuspended in 500 μL of the following buffers containing 1 m*M* PMSF: (i) 0.65 *M* sorbitol, 10 m*M* Tris-HCl, pH 7.4; (ii) 0.1 *M* $NaHCO_3$, pH 8.3; (iii) 0.1 *M* $NaHCO_3$, pH 10.0; (iv) 0.1 *M* $NaHCO_3$, pH 11.5. All samples were incubated on ice for 1 h with periodic mixing and then centrifuged at 60,000 *g* for 45 min at 4°C. The supernatants were transferred into separate tubes and subjected to TCA precipitation as described earlier. The pellets were dissolved in 50 μL of 1 × Laemmli buffer with 5% β-mercaptoethanol and incubated for 10 min at 85°C. The load control was obtained by pelleting 50 μg of gradient-purified mitochondria, which were then resuspended in 50 μL of 1 × Laemmli buffer with 5% β-mercaptoethanol.

The redox state of mitochondrial proteins was determined as described by Bode *et al.* (5) with slight modifications. Four aliquots of isolated mitochondria (50 μg/sample) were reisolated in 500 μL of 0.65 *M* sorbitol, 10 m*M* Tris-HCl, pH 7.4, 1 m*M* PMSF. Then, 60 μL of cold 100% TCA was mixed with the protein samples, followed by incubation on ice for 15 min.

The samples were centrifuged for 10 min at 20,000 *g* at 4°C. The obtained pellets were washed twice with acetone and air-dried on ice for 20 min. All pellets were resuspended within 50 μL of modifying buffer (80 m*M* Tris-HCl, pH 7.0, 10% glycerol, 2% SDS, 0.04% bromocresol green). For complete reduction of all cysteine residues, one sample was additionally treated with 2 μL of 0.5 *M* TCEP, pH 7.0. Complete oxidation was achieved by treatment with 2.5 μL of freshly prepared 100 m*M* diamide. All samples were incubated at 96°C for 15 min, followed by 5-min incubation at RT. After incubations, one sample was mock-treated with 3 μL DMSO and was used as an unmodified control. The remaining samples were treated with 3 μL of 250 m*M* mm$(PEG)_{24}$ (Thermo Fisher Scientific) and incubated for 1 h in the dark. After the treatment, the samples were resuspended in 1 × Laemmli buffer without any reactants and analyzed by nonreducing SDS-PAGE immunoblotting using 8% polyacrylamide gels.

Blue native gel electrophoretic analysis of digitonin-solubilized mitochondrial lysates produced as described earlier—except that 70 μg of mitochondria was used—was carried out by using home-made 5%–13% gradient gels as previously described (23, 41).

Immunochemical assays

Immunoprecipitation (IP) assays were conducted as previously described (19). Gradient-purified mitochondria (500 μg) were pelleted by centrifugation at 12,000 *g* for 10 min at 4°C, resuspended in 100-μL lysis buffer [1% (w/v) digitonin, 10 m*M* HEPES, pH 7.4, 50 m*M* NaCl, 2 m*M* EDTA, pH 8.0, 1 m*M* PMSF], and incubated at 4°C with gentle agitation for 15 min. The lysates were further resuspended in 1 mL of washing buffer [0.1% (w/v) digitonin, 10 m*M* HEPES, pH 7.4, 50 m*M* NaCl, 2 m*M* EDTA, pH 8.0, 1 m*M* PMSF] and spun down at 16,000 *g* for 15 min at 4°C. The supernatants were then transferred into new tubes. An aliquot of 40 μL (preprecleareance loading control) was collected. The remaining supernatants were mixed with 40 μL of preclearance IgG beads slurry (MBL International) followed by incubation at 4°C with gentle agitation for 1 h. The beads were then precipitated by a quick centrifugation at 15,000 *g* for 15 s, and clarified supernatants were transferred into new tubes. Pelleted beads were resuspended in 40 μL of lysis buffer and stored. The samples were pelleted by quick centrifugation, and the resulting supernatants were transferred into new tubes. Forty-microliter aliquots of these supernatants (postpreclearance control) were stored. The remaining supernatants were mixed with 40 μL of anti-Myc-tag magnetic beads (Santa Cruz Biotechnology) and incubated overnight at 4°C with gentle agitation. DTT (final concentration of 10 m*M*) was added to the relevant samples, whereas the other samples were left untreated. After incubation, the samples were precipitated by quick centrifugation and 40-μL aliquots of supernatants (unbound control) were collected. The beads were washed thrice with the washing buffer. Ten millimolar DTT was included in the buffer used to wash DTT-treated IP samples. After the final wash, the supernatants were transferred into a new tube and precipitated with 100 μL of ice-cold 100% TCA. The resulting protein pellets (wash controls) were resuspended in 50 μL of 1 × Laemmli buffer and incubated for 10 min at 85°C. Previously collected fractions were mixed with 8 μL of 6 × Laemmli buffer and 1 μL of 1 *M* DTT and incubated as described earlier with vigorous agitation. The final pelleted beads were resuspended in 40 μL of lysis buffer, mixed with 8 μL of DTT-supplemented 6 × Laemmli buffer, and handled as described earlier. The samples were centrifuged for 1 min at 12,000 *g*, and the resulting supernatants were transferred into new tubes and used for Western blotting by using standard 10% polyacrylamide gels.

For immunoblot analyses, gel-separated proteins were transferred onto nitrocellulose (denaturing gels) or polyvinylidene fluoride (blue native gels) membranes by tank blotting. The membranes were blocked in 5% nonfat milk in phosphate-buffered saline buffer containing 0.1% Tween-20 at room temperature and subsequently incubated with relevant primary antibodies at 4°C. The following antibodies and sera were used in this study: mouse anti-Myc epitope (11667149001, 1:1000; Roche); rabbit anti-Myc epitope (A-14, 1:2500; Santa Cruz Biotechnology); rabbit anti-FLAG epitope (2368, 1:1,000; Cell Signaling); mouse anti-Porin (459500, 1:5000; Invitrogen); mouse anti-Cox2 (ab110271, 1:2000; Abcam); rabbit anti-Aac2 (a gift from Dr. Carla Koehler, 1:5000); rabbit anti-β subunit of F_1–F_0 ATPase (a gift from Dr. Alexander Tzagoloff, 1:5000); mouse anti-Sdh1 (a gift from Dr. Dennis Winge, 1:2000); and rabbit anti-Aco1 (a gift from Dr. Roland Lill, 1:5000). The secondary horseradish peroxidase-coupled antibodies were as follows: goat anti-mouse IgG (115-035-068, 1:5000; Jackson ImmunoResearch Laboratories) and goat anti-rabbit IgG (7074S, 1:5000; Cell Signaling). The protein-antibody signals were detected by using either homemade (5 m*M* luminol, 0.4 m*M* p-coumaric acid, 100 m*M* Tris-HCl, pH 8.5 mixed with 0.2% H_2O_2 100 m*M* Tris-HCl, pH 8.5 in 1:1 proportions and used immediately) or Clarity (BioRad) chemiluminescence reagents and X-ray film (Phenix Research Products).

ATP-independent proteolytic activity

Proteolytic activity was measured by using ATP-depleted mitochondrial membranes according to the previously described procedure (24). Membranes were isolated from 300 μg of mitochondria pelleted by centrifugation at 12,000 *g* for 10 min at 4°C, resuspended in 700 μL of hypotonic 20 m*M* HEPES buffer, pH 7.4 with 1 m*M* PMSF, and subjected to gentle sonication (3 × 30 s, 50% duty cycle). Samples were centrifuged at 65,000 *g* for 1 h at 4°C. Pellets were then resuspended in 300 μL of buffer D (0.65 *M* sorbitol, 10 m*M* Tris-HCl, pH 7.4). Ten micrograms of obtained membranes were then resuspended in 200 μL of the filter-sterilized reaction buffer (10 m*M* $MgCl_2$, 50 m*M* Tris-HCl, pH 8.0, 0.05% Triton X-100) containing DTT or ascorbate. Samples were incubated at 25°C for 5 min, followed by transfer of 150 μL of the reaction mixture into a new tube containing 7.3 μL of 102.4 μM FITC-casein (Sigma-Aldrich). The samples were then incubated in the dark for 35 min with periodic mixing; finally, they were centrifuged at 20,000 *g* for 10 min at 25°C. One hundred microliters of supernatants were transferred into clear 96-well plates and used for fluorescent measurements by a Synergy 2 multi-mode microplate reader (BioTek Instruments) at 485-nm excitation and 528-nm emission wavelengths. The measurements were taken every 45 s for 10 min. The obtained measurements were exported into Microsoft Excel, used to calculate ΔA per minute, and normalized to protein concentration.

Acknowledgments

The authors thank Dr. Jennifer Fox for critical reading of the article. They thank D. Winge (University of Utah), A. Tzagoloff (Columbia University), T. Langer (University of Cologne), C. Koehler (UCLA), and S. Claypool (Johns Hopkins University) for providing reagents. This work was supported by the NIH grant GM108975 to O.K. J.V.D. was supported by the NIH training grant T32 GM107001-01A1. The content is solely the responsibility of the authors and does not necessarily represent the official views of the National Institutes of Health.

Author Disclosure Statement

No competing financial interests exist.

Supplementary Material

Supplementary Figure S1
Supplementary Figure S2
Supplementary Figure S3
Supplementary Figure S4
Supplementary Figure S5
Supplementary Table S1
Supplementary Table S2

References

1. Acin-Perez R, Lechuga-Vieco AV, DelMarMuñoz M, Nieto-Arellano R, Torroja C, Sánchez-Cabo F, Jiménez C, González-Guerra A, Carrascoso I, Benincá C, Quiros PM, López-Otín C, Castellano JM, Ruíz-Cabello J, Jiménez-Borreguero LJ, and Enríquez JA. Ablation of the stress protease OMA1 protects against heart failure in mice. *Sci Transl Med* 10: eaan4935, 2018.
2. Anand R, Wai T, Baker MJ, Kladt N, Schauss AC, Rugarli E, and Langer T. The i-AAA protease YME1L and OMA1 cleave OPA1 to balance mitochondrial fusion and fission. *J Cell Biol* 204: 919–929, 2014.
3. Baker MJ, Lampe PA, Stojanovski D, Korwitz A, Anand R, Tatsuta T, and Langer T. Stress-induced OMA1 activation and autocatalytic turnover regulate OPA1-dependent mitochondrial dynamics. *EMBO J* 33: 578–593, 2014.
4. Bode M, Longen S, Peleh V, Bihlmaier K, Dick TP, Morgan B, and Herrmann JM. Inaccurately assembled cytochrome c oxidase can lead to oxidative stress-induced growth arrest. *Antioxid Redox Signal* 18: 1597–1612, 2012.
5. Bode M, Woellhaf MW, Bohnert M, van der Laan M, Sommer F, Jung M, Zimmermann R, Schroda M, and Herrmann JM. Redox-regulated dynamic interplay between Cox19 and the copper-binding protein Cox11 in the intermembrane space of mitochondria facilitates biogenesis of cytochrome c oxidase. *Mol Biol Cell* 26: 2385–2401, 2015.
6. Bohovych I, Chan SSL, and Khalimonchuk O. Mitochondrial protein quality control: the mechanisms guarding mitochondrial health. *Antioxid Redox Signal* 22: 977–994, 2015.
7. Bohovych I, Donaldson G, Christianson S, Zahayko N, and Khalimonchuk O. Stress-triggered activation of the metalloprotease Oma1 involves its C-terminal region and is important for mitochondrial stress protection in yeast. *J Biol Chem* 289: 13259–13272, 2014.
8. Bohovych I, Fernandez MR, Rahn JJ, Stackley KD, Bestman JE, Anandhan A, Franco R, Claypool SM, Lewis RE, Chan SSL, and Khalimonchuk O. Metalloprotease OMA1 fine-tunes mitochondrial bioenergetic function and respiratory supercomplex stability. *Sci Rep* 5: 13989, 2015.
9. Calabrese G, Morgan B, and Riemer J. Mitochondrial glutathione: regulation and functions. *Antioxid Redox Signal* 27: 1162–1177, 2017.
10. Chacinska A, Pfannschmidt S, Wiedemann N, Kozjak V, Sanjuán Szklarz LK, Schulze-Specking A, Truscott KN, Guiard B, Meisinger C, and Pfanner N. Essential role of Mia40 in import and assembly of mitochondrial intermembrane space proteins. *EMBO J* 23: 3735–3746, 2004.
11. Chan DC. Fusion and fission: interlinked processes critical for mitochondrial health. *Annu Rev Genet* 46: 265–287, 2012.
12. Chen YC, Taylor EB, Dephoure N, Heo JM, Tonhato A, Papandreou I, Nath N, Denko NC, Gygi SP, and Rutter J. Identification of a protein mediating respiratory supercomplex stability. *Cell Metab* 15: 348–360, 2012.
13. Consolato F, Maltecca F, Tulli S, Sambri I, and Casari G. m-AAA and i-AAA complexes coordinate to regulate OMA1, the stress-activated supervisor of mitochondrial dynamics. *J Cell Sci* 131: jcs213546, 2018.
14. Desmurs M, Foti M, Raemy E, Vaz FM, Martinou J-C, Bairoch A, and Lane L. C11orf83, a mitochondrial cardiolipin-binding protein involved in bc 1 complex assembly and supercomplex stabilization. *Mol Cell Biol* 35: 1139–1156, 2015.
15. Diekert K, de Kroon AI, Kispal G, and Lill R. Isolation and subfractionation of mitochondria from the yeast *Saccharomyces cerevisiae*. *Methods Cell Biol* 65: 37–51, 2001.
16. Ehses S, Raschke I, Mancuso G, Bernacchia A, Geimer S, Tondera D, Martinou JC, Westermann B, Rugarli EI, and Langer T. Regulation of OPA1 processing and mitochondrial fusion by m-AAA protease isoenzymes and OMA1. *J Cell Biol* 187: 1023–1036, 2009.
17. Head B, Griparic L, Amiri M, Gandre-Babbe S, and Van Der Bliek AM. Inducible proteolytic inactivation of OPA1 mediated by the OMA1 protease in mammalian cells. *J Cell Biol* 187: 959–966, 2009.
18. Hernansanz-Agustín P, Izquierdo-Álvarez A, Sánchez-Gómez FJ, Ramos E, Villa-Piña T, Lamas S, Bogdanova A, and Martínez-Ruiz A. Acute hypoxia produces a superoxide burst in cells. *Free Radic Biol Med* 71: 146–156, 2014.
19. Herrmann JM and Westermann B. Analysis of protein-protein interactions in mitochondria. *Methods Cell Biol* 80: 743–759, 2007.
20. Ishihara N, Fujita Y, Oka T, and Mihara K. Regulation of mitochondrial morphology through proteolytic cleavage of OPA1. *EMBO J* 25: 2966–2977, 2006.
21. Jiang X, Jiang H, Shen Z, and Wang X. Activation of mitochondrial protease OMA1 by Bax and Bak promotes cytochrome c release during apoptosis. *Proc Natl Acad Sci U S A* 111: 14782–14787, 2014.
22. Käser M, Kambacheld M, Kisters-Woike B, and Langer T. Oma1, a novel membrane-bound metallopeptidase in mitochondria with activities overlapping with the m-AAA protease. *J Biol Chem* 278: 46414–46423, 2003.
23. Khalimonchuk O, Bestwick M, Meunier B, Watts TC, and Winge DR. Formation of the redox cofactor centers during Cox1 maturation in yeast cytochrome oxidase. *Mol Cell Biol* 30: 1004–1017, 2010.
24. Khalimonchuk O, Jeong MY, Watts T, Ferris E, and Winge DR. Selective Oma1 protease-mediated proteolysis of Cox1 subunit of cytochrome oxidase in assembly mutants. *J Biol Chem* 287: 7289–7300, 2012.
25. Khalimonchuk O, Ott M, Funes S, Ostermann K, Rödel G, and Herrmann JM. Sequential processing of a mitochondrial tandem protein: insights into protein import in *Schizosaccharomyces pombe*. *Eukaryot Cell* 5: 997–1006, 2006.

26. Kojer K, Bien M, Gangel H, Morgan B, Dick TP, and Riemer J. Glutathione redox potential in the mitochondrial intermembrane space is linked to the cytosol and impacts the Mia40 redox state. *EMBO J* 31: 3169–3182, 2012.
27. Korwitz A, Merkwirth C, Richter-Dennerlein R, Tröder SE, Sprenger HG, Quirós PM, López-Otín C, Rugarli EI, and Langer T. Loss of OMA1 delays neurodegeneration by preventing stress-induced OPA1 processing in mitochondria. *J Cell Biol* 212: 157–166, 2016.
28. Levytskyy R, Bohovych I, and Khalimonchuk O. Metalloproteases of the inner mitochondrial membrane. *Biochemistry* 56: acs.biochem.7b00663, 2017.
29. Levytskyy RM, Germany EM, and Khalimonchuk O. Mitochondrial quality control proteases in neuronal welfare. *J Neuroimmune Pharmacol* 11: 629–644, 2016.
30. Merdanovic M, Clausen T, Kaiser M, Huber R, and Ehrmann M. Protein quality control in the bacterial periplasm. *Annu Rev Microbiol* 65: 149–168, 2011.
31. Nishii W, Kukimoto-Niino M, Terada T, Shirouzu M, Muramatsu T, Kojima M, Kihara H, and Yokoyama S. A redox switch shapes the Lon protease exit pore to facultatively regulate proteolysis. *Nat Chem Biol* 11: 46–51, 2015.
32. Ogunbona OB, Onguka O, Calzada E, and Claypool SM. Multitiered and cooperative surveillance of mitochondrial phosphatidylserine decarboxylase 1. *Mol Cell Biol* 37: e00049-17, 2017.
33. Quirós PM, Langer T, and López-Otín C. New roles for mitochondrial proteases in health, ageing and disease. *Nat Rev Mol Cell Biol* 16: 345–359, 2015.
34. Quirós PM, Ramsay AJ, Sala D, Fernández-Vizarra E, Rodríguez F, Peinado JR, Fernández-García MS, Vega JA, Enríquez JA, Zorzano A, and López-Otín C. Loss of mitochondrial protease OMA1 alters processing of the GTPase OPA1 and causes obesity and defective thermogenesis in mice. *EMBO J* 31: 2117–2133, 2012.
35. Rainbolt TK, Lebeau J, Puchades C, and Luke Wiseman R. Reciprocal degradation of YME1L and OMA1 adapts mitochondrial proteolytic activity during stress. *Cell Rep* 14: 2041–2049, 2016.
36. Rambold AS, Kostelecky B, Elia N, and Lippincott-Schwartz J. Tubular network formation protects mitochondria from autophagosomal degradation during nutrient starvation. *Proc Natl Acad Sci U S A* 108: 10190–10195, 2011.
37. Richter U, Lahtinen T, Marttinen P, Suomi F, and Battersby BJ. Quality control of mitochondrial protein synthesis is required for membrane integrity and cell fitness. *J Cell Biol* 211: 373–389, 2015.
38. Sakowska P, Jans DC, Mohanraj K, Riedel D, Jakobs S, and Chacinska A. The oxidation status of Mic19 regulates MICOS assembly. *Mol Cell Biol* 35: 4222–4237, 2015.
39. Wai T, García-Prieto J, Baker MJ, Merkwirth C, Benit P, Rustin P, Rupérez FJ, Barbas C, Ibañez B, and Langer T. Imbalanced OPA1 processing and mitochondrial fragmentation cause heart failure in mice. *Science* 350: aad0116-aad0116, 2015.
40. Weckbecker D, Longen S, Riemer J, and Herrmann JM. Atp23 biogenesis reveals a chaperone-like folding activity of Mia40 in the IMS of mitochondria. *EMBO J* 31: 4348–4358, 2012.
41. Wittig I, Braun HP, and Schägger H. Blue native PAGE. *Nat Protoc* 1: 418–428, 2006.
42. Xie JL, Bohovych I, Wong EOY, Lambert J-P, Gingras A-C, Khalimonchuk O, Cowen LE, and Leach MD. Ydj1 governs fungal morphogenesis and stress response, and facilitates mitochondrial protein import via Mas1 and Mas2. *Microb Cell* 4: 342–361, 2017.
43. Zhang K, Li H, and Song Z. Membrane depolarization activates the mitochondrial protease OMA1 by stimulating self-cleavage. *EMBO Rep* 15: 576–585, 2014.

Address correspondence to:
Dr. Oleh Khalimonchuk
Department of Biochemistry
University of Nebraska-Lincoln
1901 Vine Street N230 BEAD
Lincoln, NE 68588-0664

E-mail: okhalimonchuk2@unl.edu

Date of first submission to ARS Central, September 13, 2018; date of final revised submission, April 3, 2019; date of acceptance, May 1, 2019.

Abbreviations Used

AAA = ATPase associated with various cellular activities
BN-PAGE = blue native gel electrophoresis
CCCP = carbonyl cyanide m-chlorophenyl hydrazone
coIP = co-immunoprecipitation
DTT = dithiothreitol
EDTA = ethylenediaminetetraacetic acid
FITC = fluorescein isothiocyanate
H_2O_2 = hydrogen peroxide
IM = inner mitochondrial membrane
IMS = mitochondrial intermembrane space
IP = immunoprecipitation
m-AAA = matrix-oriented AAA
$mm(PEG)_{24}$ = methyl-polyethylene glycol maleimide 24
NaCl = sodium chloride
PMSF = phenylmethylsulfonyl fluoride
qRT-PCR = quantitative real-time polymerase chain reaction
SDS-PAGE = sodium dodecyl sulfate–polyacrylamide gel electrophoresis
TCA = trichloroacetic acid
TCEP = tris(2-carboxyethyl)phosphine
UPS = ubiquitin-proteasome system
WT = wild type